Mechanism of ultra low friction of multilayer graphene studied by coarse-grained molecular simulation

Hitoshi Washizu,*[a] Seiji Kajita,[a] Mamoru Tohyama,[a]
Toshihide Ohmori,[a] Noriaki Nishino,[b] Hiroshi Teranishi[b]
and Atsushi Suzuki[b]

Coarse-grained Metropolis Monte Carlo Brownian Dynamics simulations are used to clarify the ultralow friction mechanism of a transfer film of multilayered graphene sheets. Each circular graphene sheet consists of 400 to 1,000,000 atoms confined between the upper and lower sliders and are allowed to move in 3 translational and 1 rotational directions due to thermal motion at 300 K. The sheet–sheet interaction energy is calculated by the sum of the pair potential of the sp2 carbons. The sliding simulations are done by moving the upper slider at a constant velocity. In the monolayer case, the friction force shows a stick-slip like curve and the average of the force is high. In the multilayer case, the friction force does not show any oscillation and the average of the force is very low. This is because the entire transfer film has an internal degree of freedom in the multilayer case and the lowest sheet of the layer is able to follow the equipotential surface of the lower slider.

1 Introduction

Lamellar materials, such as graphite, often show low friction in air. Graphite and molybdenum disulfide are typical low friction materials, while mica is not.[1] These materials are used as solid lubricants in an artificial satellite in which liquid lubricants, such as hydrocarbons, are not used because of the high vacuum environment. Some additives are mixed into automotive lubricants in order to generate a solid lubricant film in the sliding contact area due to the heat and shear which often undergo tribochemical reactions.[2]

The mechanism of low friction in such lamellar materials, whether the interlayer actions are due the van der Waals interactions or Coulomb ion pair interactions, is commonly explained by the slip generated between the layers. When we put the pile of papers on the desk and slide the uppermost paper, it appears that the inner paper slipping generates the low friction. However, this macroscopic mechanism is not confirmed to occur in the nanoscopic range.

Assume that a steel ball with a radius of several millimetres is sliding on an infinitely long graphene[3] sheet on the graphite. In this case, the graphene cannot slide as the pulling force will be infinitely high when the pulling force is finite per unit length. The effect of bending should also be considered in the realistic case as the shearing between the layers is hard to put into practice for geometrical reasons.

[a]*Toyota Central R&D Labs., Inc., Nagakute, Aichi 480-1192, Japan. E-mail: h@washizu.org;
Fax: +81 561 63 6920; Tel: +81 561 71 7531*
[b]*Toyota Motor Corporation, 1 Toyota-cho, Toyota, Aichi 471-8572, Japan*

To consider the realistic phenomena, the low friction should be due to the sliding motion between the small pieces of graphene layers which are transferred to the steel ball and the lower substrate graphite. The surface has a roughness of a micron order and the transfer film is assumed to be physically adsorbed. Some transfer films are visualized by a Transmission Electron Microscope.[4] Recently, the molecular dynamics simulations concerning interactions between a graphite surface and the rigid pyramidal nanoasperity have shown the cleavage and flake formation of graphite.[5]

The question is then the mechanism of friction between the transfer film and the graphite surface. Does the friction occur inside the transfer film similar to the macroscopic friction of the pile of papers? If not, what is the difference in the friction mechanism between general solid materials and lamellar materials? In general crystal materials, sliding between the same materials produces a high friction.[1] The case of low friction is attributed to the incommensurate systems in which the rotation (yaw) angles of two surfaces are twisted.[6,7] The physically adsorbed transfer film may rotate in a commensurate condition for a long time due to the stability of the thermal equilibrium structure. Therefore, the macroscopically observed low friction of lamellar materials is not totally understood from the viewpoint of an incommensurate friction mechanism.

From a molecular point of view, the most underlying problem when investigating these phenomena is the size of the transfer film. The transfer film consists of a huge number of atoms[4] which is difficult to treat by an atom based simulation, such as molecular dynamics (MD) or molecular mechanics (MM). Based on this difficulty, MD and MM simulations are either performed for a small flake of graphene,[8,9] or for an infinitely large sheet by adopting periodical boundary conditions.[10] A coarse-grained molecular simulation is needed to overcome this difficulty.

The transfer film consists of graphene sheets. One concept is to model each graphene sheet as a rigid body. The covalent bond of the carbon atoms is on the order of 100 $k_B T$ and the van der Waals interlayer interaction is on the order of $k_B T$,[11] where T is the absolute temperature and k_B is the Boltzmann constant. This can be one foundation to support such a rough molecular model. Each graphene sheet has several internal vibration modes. The fluctuation of the sp2 electron cloud due to this internal vibration can be the source of the thermal fluctuation of the van der Waals force which affects the thermal motion of neighboring graphene sheets. The rigid body has 3 translational and 3 rotational degrees of freedom. The important degrees of freedom are the 3 translational and yaw rotational angles which are the motion around the axis in the direction of the film thickness. Based on these assumptions, the sliding dynamics of a transfer film can be described as the motion of a set of rigid graphene sheets which move by thermal brownian motion in 4 degrees of freedom.

In this study, coarse-grained Metropolis Monte Carlo Brownian dynamics (MCBD)[12–14] simulations are employed to investigate the friction dynamics of the transfer film of multilayered graphene sheets. MCBD was first introduced by Kikuchi et al.[12] in order to calculate the dynamics of colloid suspensions. This method is mathematically the same as Langevin dynamics, but has advantages in calculation stability and speed. MCBD is suitable for a system for which the effect of the thermal fluctuation and the inner sheet interactions are comparable in order.

2 Simulation method

2.1 Monte Carlo Brownian dynamics

The MCBD is the numerical solver of the Fokker–Plank diffusion equation and physically equal to the Langevin dynamics.

The Metropolis Monte Carlo (MC) method,[15] when applied to part of the degrees of freedom of a system, e.g., the center of graphene sheets, turns into a simulation

procedure for the Brownian motion of the sheets. The Metropolis MC was originally developed as a method for calculating statistical mechanical configuration integrals. Since the MC sampling is a Markovian process, if we introduce a "time" scale t which actually labels the order of subsequent configurations X, the "dynamic" evolution of the probability distribution function is governed by the master equation[16]

$$\frac{\partial P(X,t)}{\partial t} = \int \left\{ W(X|X'X')P(X',t) - W(X'|X)P(X,t) \right\} dX' \tag{1}$$

where $W(X|X')$ is the transition probability per unit "time" for a transition from configuration X' to X. The master equation may be approximately solved by an expansion method in powers of a parameter Ω, the size of the system. Given that $W(X|X')$ has the canonical form

$$W(X|X') = \Phi_0(x';r) + \Omega^{-1}\Phi_1(x';r) + \Omega^{-2}\Phi_2(x';r) + \ldots \tag{2}$$

with $x' = X'/\Omega$ and $r = X - X'$, the jump moments are defined by

$$\alpha_{\nu,\lambda}(x) = \int r^\nu \Phi_\lambda(x;r)dr \tag{3}$$

When $\alpha_{1,0} = 0$, the Ω expansion yields the lowest approximation of a nonlinear Fokker–Planck equation:

$$\frac{\partial P(X,\tau)}{\partial \tau} = -\frac{\partial}{\partial x}\alpha_{1,1}(x)P + \frac{1}{2}\frac{\partial^2}{\partial x^2}\alpha_{2,0}(x)P \tag{4}$$

with $\tau = \Omega^{-2}t$. In the Metropolis MC, the reciprocal of the maximum displacement allowed for an MC move during a "time" interval Δt may be taken as the parameter Ω. The transition probability then has the canonical form with

$$\Phi_0(x;r) = \frac{1}{2\Delta t} \quad \text{for} \quad |r| \leq 1$$
$$\text{and} \qquad = 0 \quad \text{for} \quad |r| > 1$$

and, supposing, for example, the derivative of the potential energy of the system $U(x)$ with respect to x is negative, i.e., $U(x) < 0$, with

$$\Phi_1(x;r) = -\frac{1}{2k_B\Delta t}U'(x)r \quad \text{for} \quad -1 \leq |r| < 0$$
$$\text{and} \qquad = 0 \quad \text{for} \quad r < -1 \quad \text{and} \quad r \geq 0$$

for a sufficiently large Ω. From these one obtains

$$\alpha_{1,0} = 0, \alpha_{2,0} = \frac{1}{3\Delta t}, \alpha_{1,1} = -\frac{1}{2N_f k_B T \Delta t}U'(x) \tag{5}$$

where N_f is the number of the degree of freedom, so that eqn (4) reduces to the diffusion equation

$$\frac{\partial P(X,t)}{\partial t} = \frac{D}{k_B T}\frac{\partial}{\partial x}U'(x)P + D\frac{\partial^2}{\partial x^2}P \tag{6}$$

where the diffusion constant D is defined by

$$2N_f D\Delta t\Omega^2 = 1 \tag{7}$$

Thus, by making the size of the maximum allowed displacement Ω^{-1} in the Metropolis MC very small the forces acting on a particle remain essentially constant during

the Monte Carlo "time" step, the method turns into a Brownian dynamics simulation.

The merit of MCBD compared to a molecular dynamics based simulation is that the calculation of the forces acting on each sheet is not needed and only the calculation of the potential energy $U(x)$ is needed so that the calculation remains stable. Compared to the general Monte Carlo method, MCBD provides the time evolution of a physical quantity, where averaging of multiple trajectories is needed.

As described above, the reality of the MCBD simulation relies on the reality of the interacting energy $U(x)$ and the diffusion coefficients D. In this paper, we constructed $U(x)$s from a widely used pairwise potential parameter proposed by Girifalco *et al.*[17] The potential is used in sp2 carbons, such as graphites, carbon nanotubes, and C60 and evaluated in elastic and thermal properties. In order to obtain the diffusion coefficients, D, ether experiments and atom-based simulations are available. The parameters can be more precisely obtained from *ab initio* quantum calculations.

2.2 Potential between graphene sheets

In the structure of graphites under a thermal equilibrium stable AB stuck structure, the distance between carbon atoms l_a is 1.42 $\overset{\circ}{A}$, and the average distance between sheets l_z is 3.35 $\overset{\circ}{A}$. The interaction between graphene sheets calculated and stored during the simulation are taken from the literature.[17] This potential reproduces the stable AB stuck structure and the stress during separation of the two graphene sheets. Using this pairwise potential for the interactions between rigid sheets, the anisotropy of potential landscape due to the motion of sheets is obtained.

The potential between the sp2 carbon atoms $U_{\text{atom–atom}}(r_a)$ is described by the following Lennard–Jones type function

$$U_{\text{atom–atom}}(r_a) = -\frac{A}{r_a^6} + \frac{B}{r_a^{12}} \tag{8}$$

where r_a is the distance between carbon atoms, A and B are constants. This function can be written using the parameter which describes the depth of the potential ε and the equilibrium distance σ.

$$U_{\text{atom–atom}}(r_a) = 4\varepsilon\left[-\left(\frac{\sigma}{r_a}\right)^6 + \left(\frac{\sigma}{r_a}\right)^{12}\right] \tag{9}$$

ε, and r_{a0} are rewritten as follows:

$$\varepsilon = \frac{A^2}{4B}, \tag{10}$$

$$r_{a0} = 2^{1/6}\sigma = \left(\frac{2B}{A}\right)^{1/6}. \tag{11}$$

We used the pairwise inter atom potential on the graphene sheets as A = 15.2 eV $\overset{\circ}{A}^6$, B = 24.1 × 10⁻³ eV $\overset{\circ}{A}^{12}$, r_0 = 3.83 $\overset{\circ}{A}$, ε = 2.89 meV.

We then calculated the potential between a carbon atom and a graphene sheet by the following equation using eqn (8).

$$U_{\text{atom–sheet}}(x,y) = \sum U_{\text{atom–atom}}(r_a) \tag{12}$$

We set x as the sliding direction in Cartesian coordinates, y as the perpendicular direction to the sliding direction, and the summation at the rhs as the sum of the interactions between a set of carbon atoms in a honeycomb structure of unit

length l_a in the $z = 0$ plane and a carbon atom at $z = \Delta z$. During the simulation, we employed the coordinate system based on the vectors $a = ((\sqrt{3}/2)l_a, (1/2)l_a), b = (0, l_a)$ considering the symmetry and calculated $U_{\text{atom–sheet}}$ before the simulation on the lattice point divided by 100 in the a,b directions, and returned to the Cartesian coordinates during the motion of the sheets in order to calculate the potential energy between the sheets.

Each $U_{\text{atom–sheet}}$ on the lattice points are calculated until the difference in the energy converges to $\Delta U_{\text{atom–sheet}} < 10^{-6}$ eV from the neighbor to farther atoms. Fig. 1 shows the $U_{\text{atom–sheet}}(x,y)$ in the Cartesian coordinates.

As two carbon atoms, which are facing each other on the honeycomb structures, can be geometrically distinguished by the periodicity, the potential between the sheets $U_{\text{sheet–sheet}}$ is calculated using $U_{\text{atom–sheet}}(x, y)$.

$$U_{\text{sheet–sheet}} = (U_{\text{atom–sheet}}(\Delta x, \Delta y) + U_{\text{atom–sheet}}(\Delta x, \Delta y - (1/2)l_a)) \cdot S(\Delta x, \Delta y) \quad (13)$$

where Δx and Δy are the distances between center of two circle shaped sheets in the x and y directions respectively, and $S(\Delta x, \Delta y)$ is the number of the carbon atoms in an overlapped area of two circles in a position Δx and Δy. By eqn (13), the end effect which is the effect of the finite size of the graphene sheets is able to be included in the simulation. The potential surface $U_{\text{sheet–sheet}}$ of the system is plotted in Fig. 2. $\Delta x = 0$ and $\Delta y = 0$ correspond to the AB stuck structure and the interaction between the sheets decreases when two sheets are in separated positions.
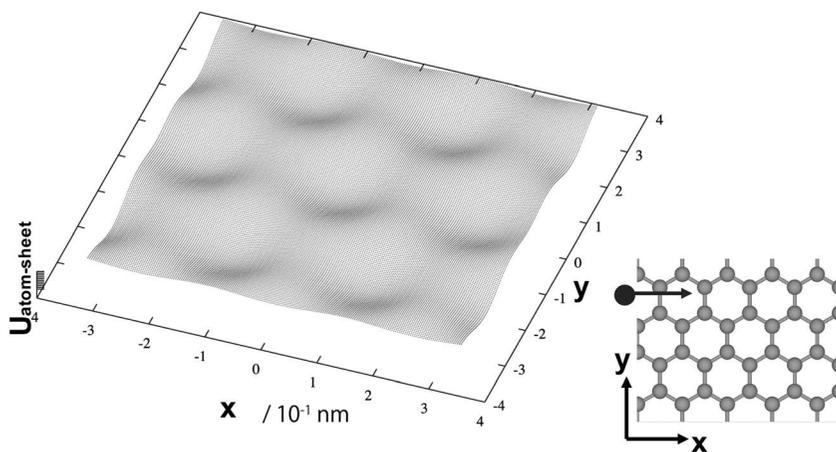
Fig. 1 Potential between a carbon atom and a graphene sheet $\Delta U_{\text{atom–sheet}}$ (x,y plane).
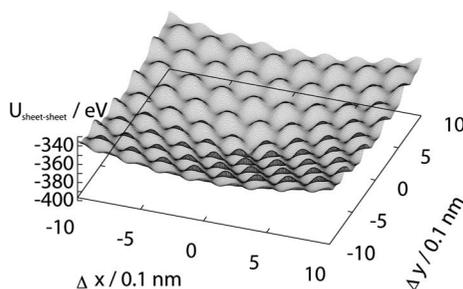
Fig. 2 Potential between two graphene sheets $\Delta U_{\text{sheet–sheet}}$ (x, y plane).

The interaction between a graphene sheet and an infinitely large graphite plate $U_{sheet–plate}$ is described as follows:

$$U_{sheet–plate} = (U_{atom–sheet}(x,y) + U_{atom–sheet}(x,y - (1/2)l_a)) \cdot N_{xy}/2 \qquad (14)$$

where x,y are the coordinates of the sheet, and N_{xy} is the number of atoms in the sheet. During this interaction, the inclined baseline shown in Fig. 2 does not exist and the potential becomes a periodical function.

The effect of the incommensurate surface interaction is included by adopting a smooth energy surface when two sheets are twisted at the yaw angle θ. The effect of the yaw angle is included as follows. The potential between graphene sheets $U_{sheet–sheet}$ is set to an average value $U_{sheet–sheet} = U_{ave}$ when the difference between the sheet rotation angles becomes 0.1 degree. In Fig. 3, this simulation condition is plotted using the direct calculation due to the interactions of the finite number of carbon atoms. Although the direct calculation shows cyclic functions, this effect is neglected for simplicity.

For the z direction, which is the direction of load and the film thickness, each potential energy is already calculated $U_{sheet–sheet}(x,y)$ as a summation of each atom pair potential $U_{atom–sheet}$ for the distance between both sheets Δz. During the simulations, $U_{sheet–sheet}(x,y)$ is stored as a table calculated before the MC simulation run starts. The values of $U_{sheet–sheet}(x,y)$ is linearly complemented from the mesh value.
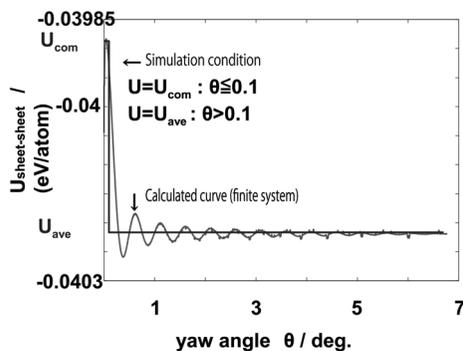
Fig. 3 Potential between two graphene sheets $\Delta U_{sheet–sheet}$ as a function of the yaw angle θ.
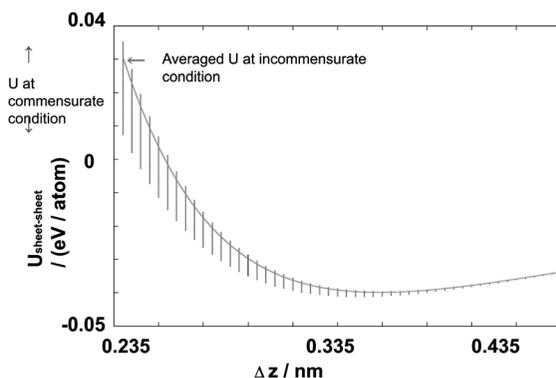
Fig. 4 Potential between two graphene sheets $U_{sheet–sheet}$ as a function of z.

Fig. 4 shows the sheet potential $U_{sheet-sheet}$ as a function of Δz under a commensurate condition. The averaged U under the incommensurate condition is also plotted as a curve. Each bar shows the range of the $U_{sheet-sheet}$ distribution in the (x, y) plane. A small Δz corresponds to a high pressure under a heavy load which shows a large range of energy in the commensurate condition. As Δz increases, which corresponds to a lower pressure, the range of $U_{sheet-sheet}$ decreases and when over the equilibrium width of 0.335 nm, $U_{sheet-sheet}$ does not significantly change.

2.3 Simulation conditions

The MCBD simulation conditions are described as follows. Each circular graphene sheets consist of 400 ($N_{xy} = 20 \times 20$) to 1 000 000 ($N_{xy} = 1\,000 \times 1\,000$) atoms allowed to move in 3 translational and 1 rotational directions due to thermal motion at 300 K. The transfer layer consists of N_z graphene sheets piled in the z direction.

The initial conditions of the graphene sheets are set for the AB stuck structure at the origin and confined by the upper and lower sliders. The lower slider is set to an infinitely wide plane. The interaction between the lowest confined graphene sheet and the lower slider is set to the same interaction without the end effect. The upper slider is fixed to the same size as the confined graphene sheets. The interaction between the top confined graphene sheet and the upper slider is set to the same interaction including the end effect. The effect of the load in the z direction is given by setting the total width of the upper and the lower sliders to a fixed value $l_z \times (N_z + 1)$ where $l_z = 0.330$ nm is the average of the interlayer distance.

The sliding simulation is done by moving the upper slider in the x direction 1.0×10^{-8} nm MC^{-1} step. In the heaviest case $N_{xy} = 1\,000 \times 1\,000$, $N_z = 1$, the number of atoms is 1 000 000 which may take a huge amount of time for an all atom molecular dynamics simulation. In this method, the total simulation time depends on N_z and not on N_{xy} due to the calculation method described in the former subsection *i.e.*, we first calculate the potential table $U_{atom-sheet}$ in the infinite system, then calculate $U_{sheet-sheet}$ by multiplying the number of atoms N_{xy} including the end effect. The radius of the transfer film on $N_{xy} = 100 \times 100$, $N_z = 10$ is equivalent to the flake diameter of 18.2 nm and thickness of 3.7 nm which is almost as the same scale as the transfer film observed on the AFM tip.[4]

The maximum allowed displacement is set to $\Omega_x^{-1} = \Omega_y^{-1} = 0.01$ Å for the x, y direction, $\Omega_z^{-1} = 0.001$ Å for the z direction and $\Omega_\theta^{-1} = 0.01$ for the θ direction. Each Monte Carlo time step in the MCBD method and physical time Δt is related to using the diffusion coefficient D in eqn (4). Although the correlations between the directions of fluctuations are assumed to be independent in this study, the correlation between the x, y directions should be considered in the future.

3 Results and discussions

The sliding simulations are done by moving the upper slider at a constant velocity. Fig. 5 shows the typical time developments of the x coordinates of the graphene sheets. As the upper slider moves in the x direction, the graphene sheets follows the upper slider. The lower the sheet number N_z, the larger the delay in the motion of the sheets and the curve shows a wavy pattern.

The trajectory during the sliding motion of the lowermost sheet $N_z = 10$ is plotted *vs.* the potential surface between the lower slider and the 10th sheet in Fig. 6. It is clearly shown that even the upper slider moves against the potential hill, and the lowest sheet slides toward the valley of the potential surface. More precisely, a stay motion at the bottom of the potential surface is also shown. Apart from the stay, the trajectory shows that the motion of the lowermost sheet is almost on the plane energy surface.

Time development of the friction forces $F_x = \Delta U / \Delta x$ is plotted in Fig. 7 for $N_z = 1$ and $N_z = 10$, where ΔU is the difference in the total potential energy of transfer film
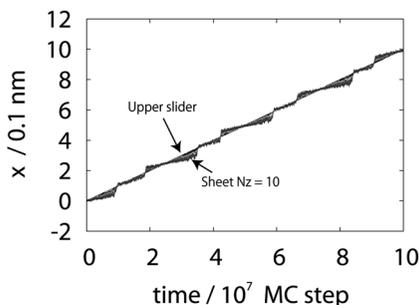
Fig. 5 Motion of each graphene sheet in x direction under sliding condition. The lowest curve is the 10th layer. $N_{xy} = 10,000$, $N_z = 10$, Degrees of freedom: x,y,z,θ, $l_z = 0.330$ nm.
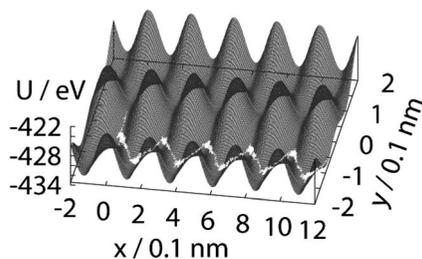
Fig. 6 Trajectory of the center of the 10th sheet of the transfer layer and the potential surface between the lower slider and the 10th sheet.

and Δx is the motion in the x direction. In the $N_z = 1$ system, the stick-slip like oscillation of the friction force is found. On the other hand, in the $N_z = 10$ system, the friction force fluctuates around zero and no oscillation is found. This is due to the motion shown in Fig. 6 that the lowest sheet moves the plane, which is almost equal to $\Delta U = 0$, and the friction force, which is calculated from this quantity, becomes very small. We call this motion of multilayer graphene sheets which generates a low friction as the thermal escaping motion.

In order to quantitatively discuss the low friction force due to the thermal escaping motion, the averaged friction forces F_x in several N_{xy} and N_z are plotted in Fig. 8. When the sheets are large enough ($N_{xy} \geq 60^2$), the large friction force F_x is found when $N_z = 1$ and decreases when $N_z > 1$ which is due to the thermal escaping motion. The friction force F_x increases as the number of N_{xy} increases when $N_z = 1$. The friction force F_x slightly increases as N_z increases in $N_z \geq 3$ and does not show any sheet size N_{xy} dependence. This may be due to the friction between the inner sheets; in other words, the weakening of the spring constant of a whole transfer film. When the sheets are small ($N_{xy} \leq 40^2$), the friction forces monotonously increase with the increase in N_z and the two curves are different in $N_z \geq 3$ which suggests the lack of any thermal escaping motion.

Considering the mechanism of the thermal escaping motion, a conceptual illustration is shown in Fig. 9. The confined graphene sheet interacts with both the upper slider and the lower slider shown in Fig. 9(a). When the upper slider moves right, the interaction region of the upper side decreases whereas the lower side does not change. The graphene sheet moves in the right direction in order to compensate for the lost interacting region and the stability recovers (Fig. 9(b)). This is the end effect which is the basic reason that the graphene sheet follows the upper slider. In other words, an asymmetric situation due to the existence of the ends of the upper and the lower sliders makes the basic motion. In realistic sheets, the potential energy
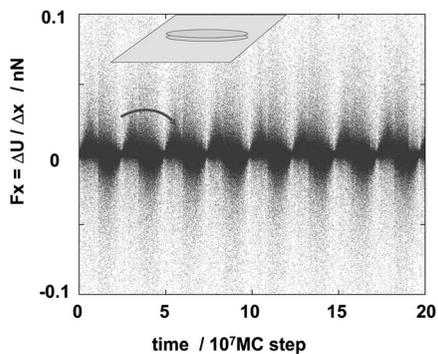
(a)
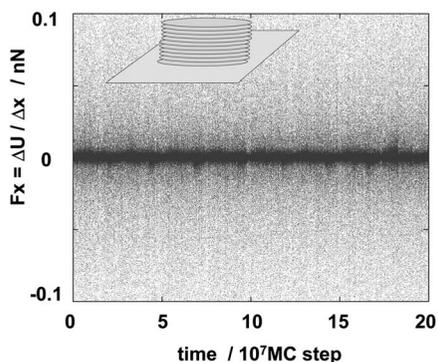
(b)

Fig. 7 Time development of the friction force for a number of sheets $N_z = 1$ (a), $N_z = 10$ (b).
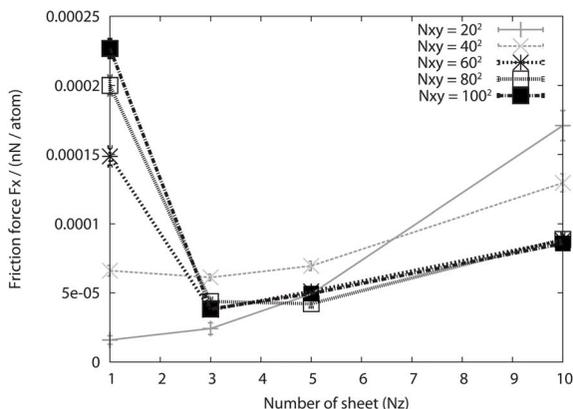
Fig. 8 Dependence of the size of the sheets (N_{xy}), the number of sheets (N_z) on friction force F_x. The friction force is averaged by the MCBD simulation of 2×10^8 MC step at 16 calculations under independent initial conditions. The error bars are almost within the size of the markers.

function drawn in Fig. 9(b) has the landscape precisely shown as $U_{sheet–sheet}$ in Fig. 3 which has local minima (Fig. 9(c)). In order to move out from the local minima, thermal fluctuation is necessary. This is strongly related to the size N_{xy} and number of sheets N_z dependence on the friction force F_x found in Fig. 8.
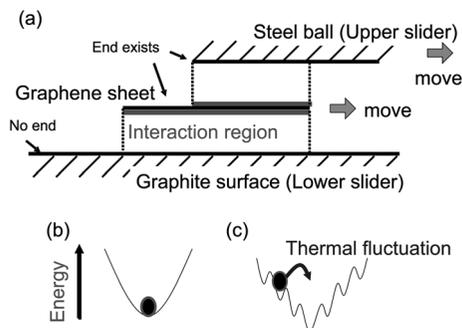
Fig. 9 A conceptual illustration of the end effect.

The trajectories on the xy plane under the three different sheet numbers $N_z = 1, 3,$ 10 are plotted in Fig. 10. In the $N_z = 1$ system, because of the restricted free lateral motion, the trajectory is narrow in the y direction and the graphene sheet climbs the potential hill. In the $N_z = 3, 10$ systems, the widths of the fluctuation range in the y direction are almost the same and thermal escape is found. Note that due to the stochastic motion of the sheets, the sheets randomly move both positively and negatively in the y direction when $N_z = 3, 10$.

From an energetic point of view, the time evolution of the total energy U_t of the three different sheet numbers $N_z = 1, 3, 10$ are plotted in Fig. 11. In the $N_z = 3, 10$ systems, the fluctuation of U_t is very small and almost used as a single quantity. In the $N_z = 1$ system, the U_t separates into two quantities and the fluctuation of each quantity is high. This means that when $N_z = 1$, the confined graphene sheet must move to two stable points which are made by the upper and lower sliders. The binary energy difference ΔU_B is about 20 meV and the transfer motion between the two stable points generates a large hysteresis which causes a high energy dissipation. The increase in the friction force F_x on N_{xy} when $N_z = 1$ shown in Fig. 8 can be explained from this point of view, *i.e.*, the increase in ΔU_B causes an increase in the friction.

The friction behavior of a small flake of a sheet ($N_{xy} = 20^2, 40^2$) shown in Fig. 8 is different compared to that of a larger sheet. This can be understood by the thermal fluctuation. Fig. 12 shows the fluctuation of the total energy U_t for different sheet sizes N_{xy}. In the $N_{xy} = 20^2$ system, it shows a very large fluctuation with the range $\Delta U_t = 0.5$ meV. For $N_{xy} = 40^2$, it also show a large fluctuation which is smaller than the $N_{xy} = 20^2$ system whereas the larger system shows almost the same range of fluctuation. In the $N_{xy} = 20^2$ system, it does not show any oscillation of the energy which
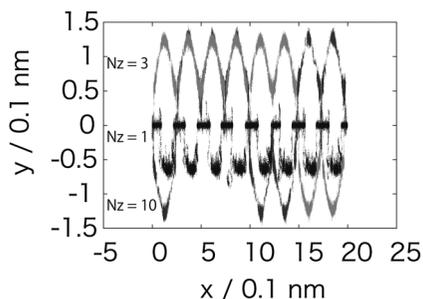
Fig. 10 The trajectories on xy plane under three different sheet numbers N_z ($N_{xy} = 100^2$). Each sheet moves from the origin at time $t = 0$ to the positive direction of the x axis.
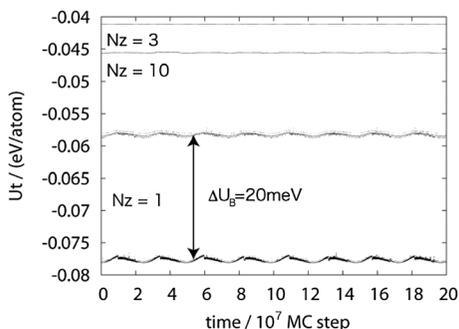
Fig. 11 The time evolution of the total energy U_t of the three different sheet numbers N_z ($N_{xy} = 100^2$).
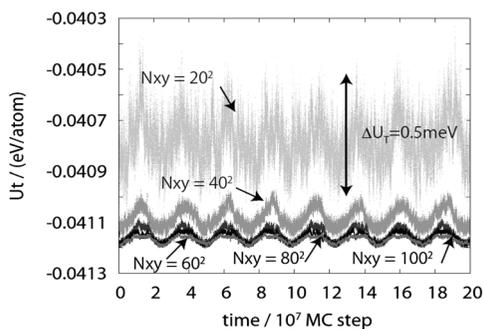
Fig. 12 The time evolution of the total energy U_t of the five different sheet sizes N_{xy} ($N_z = 10$).

is found in the others. This means that in the $N_{xy} = 20^2$ system, the thermal fluctuation exceeds the depth of the periodical potential well in the potential landscape of the lowermost sheet and the lower slider. A sufficient depth of the potential well is needed to stick the graphene sheets together. For this reason, the small sheets cannot exhibit the thermal escape motion found in the larger sheet systems.

In contrast, when the sheet size is very large, the depth of the potential well in each graphite interaction exceeds the thermal fluctuation. The friction behavior of a very large system $N_{xy} = 1\,000^2$ is plotted in Fig. 13 with the potential surface of the potential between the sheet and the lower slider. When compared to the trajectory for $N_{xy} = 100^2$ shown in Fig. 10, the motion in the y direction is completely suppressed and the sheet climbs the potential hill. In this case, the friction may be due to the energy dissipation of the atom vibration. This is same as in the case for phonon dissipation in general solid materials.[18,19]

Using the coarse-grained Metropolis Monte Carlo Brownian Dynamics simulations, we found a low friction behavior in multilayer graphene sheets which we called the thermal escape motion. The low friction of lamellar materials has been explained by the weak interaction between the layers. However, even if the interaction is weak in a commensurate system, the atoms must overcome the potential hill which produces a large energy dissipation.[18,19] Note that the van der Waals interaction energy is on the same order for the graphite sp2 carbon and the other elements. The weakness of the interlayer bond in the depth direction should cause a weak spring constant, then the energy dissipation becomes high. Therefore, we cannot directly understand the low friction of lamellar materials from this point of view.
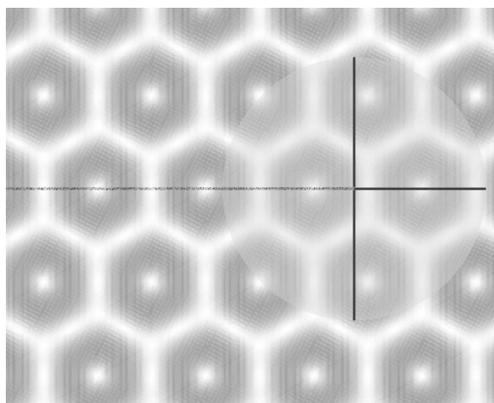
Fig. 13 Trajectory of the very large single sheet ($N_{xy} = 1\,000^2$, $N_z = 1$).

The largest difference between general solid materials and lamellar materials is that, in the transfer film of lamellar materials, each sheet has high translational and rotational degrees of freedom. Due to the flexibility of the whole transfer film by this degree of freedom, the sheet can escape the potential hills. This is the only situation for the multilayer case already shown in our simulation. This motion also occurs only when the potential well depth and the degree of thermal fluctuation are comparable. If the thermal fluctuation is high in a small flake, the upper slider cannot hold the film. If the potential well depth is high in the very large sheet, the sheets cannot escape the potential hill by thermal fluctuation. This thermal escape motion has not been reported as far as the authors know by a study using an all-atom simulation such as MD or MM. This can be explained by the restriction of the MD or MM the precise simulation can treat a very small flake,[8,9] or infinitely large sheet by adopting periodic boundary conditions.[10]

The total friction force due to the sliding is the sum of the energy dissipation due to the atomistic lattice vibration[18,19] and the energy dissipation due to the conformational change in the entire transfer film which is calculated in this paper. To compare it with the experiments, the effect of the atomistic lattice vibration should be included for a precise discussion. We have, however, already found the difference between the single layer and the multilayer case for the amount of energy dissipation due to the conformational change. By including the atomistic lattice vibration, the thermal escaping motion will decrease the impulse of atoms on the opponent surface so that the difference between the single and the multilayer case will become larger.

Our simulation also shows that the very low friction of the lamellar materials is able to exist even in the commensurate system. We think that the low friction of the lamellar materials obtained from macroscopic experiments can be explained by this mechanism.

The effects of the chemical nature at the edge[20] are not included in our rough simulation. Also, the effect of a vacancy and defect are not included.[21] In another study, these can be treated using a modified potential surface. The effect of the internal atom vibration should also be studied by using direct all-atom simulations. In these means, the all-atom simulations and our coarse-grain simulation are complementary in each other. A comparison with the experiments is also desired. This can be realized by fixing the size and the number of graphene sheets on the atomistic friction experiments such as by the atomistic force microscope. Recently, the friction of a fixed number of graphene sheets was measured,[22–24] whereas the size of the sheets was obviously larger than the transfer film which is our concern. We would verify the mechanism for the thermal escape motion by measuring the friction force of a transfer film for a fixed size and number of graphene sheets.

4 Conclusions

The Monte Carlo Brownian Dynamics simulation was used to investigate the friction motion for a transfer layer of graphite. In the monolayer case, the friction force showed a stick-slip like curve and the average of the force was high. In the multilayer case, the friction force did not show any oscillation and the average of the force was very low. This is because the entire transfer film obtained the internal degree of freedom in the multilayer case and the lowest sheets of the layer were able to follow the equipotential surface of the lower slider which is called the thermal escape motion. The low friction of lamellar materials obtained in macroscopic experiments is able to be explained by this mechanism.

Acknowledgements

References

1 F. Bowden and D. Tabor, in *The friction and lubrication of solids*, Oxford: Clarendon Press, Oxford, 1964.
2 A. Erdemir and E. J.-M. Martin, in *Superlubricity*, Elsevier Science, Amsterdam, 2007.
3 A. Geim and K. Novoselov, *Nat. Mater.*, 2007, **6**, 183.
4 M. Dienwiebel, *et al.*, *Surf. Sci.*, 2005, **576**, 197.
5 A. Khomenko and N. Prodanov, *Carbon*, 2010, **48**, 1234.
6 M. Hirano and K. Shinjo, *Phys. Rev. B: Condens. Matter*, 1990, **41**, 11837–11851.
7 K. Shinjo and M. Hirano, *Surf. Sci.*, 1993, **283**, 473–478.
8 N. Sasaki, K. Kobayashi and M. Tsukada, *Phys. Rev. B: Condens. Matter*, 1996, **54**, 2138–2149.
9 G. S. Verhoeven, M. Dienwiebel and J. W. M. Frenken, *Phys. Rev. B: Condens. Matter Mater. Phys.*, 2004, **70**, 165418.
10 N. Itamura, K. Miura and N. Sasaki, *Jpn. J. Appl. Phys.*, 2009, **48**, 060207.
11 Israelachvili, in *Intermolecular and Surface Forces*, Third Edition, Academic Press, Burlington, 2010.
12 K. Kikuchi, M. Yoshida, T. Maekawa and H. Watanabe, *Chem. Phys. Lett.*, 1991, **185**, 335–338.
13 H. Washizu and K. Kikuchi, *J. Phys. Chem. B*, 2002, **106**(43), 11329.
14 H. Washizu and K. Kikuchi, *J. Phys. Chem. B*, 2006, **110**(6), 2855–2861.
15 N. Metropolis, A. W. Rosenbluth, M. N. Rosenbluth, A. H. Teller and E. Teller, *J. Chem. Phys.*, 1953, **21**, 1087–1092.
16 N. G. van Kampen, in *Stochastic processes in physics and chemistry*, revised and enlarged edition, North-Holland, Amsterdam, 1992, ch. 11.
17 L. Girifalco, M. Hodak and R. S. Lee, *Phys. Rev. B: Condens. Matter*, 2000, **62**, 13104.
18 S. Kajita, H. Washizu and T. Ohmori, *Europhys. Lett.*, 2009, **87**(6), 66002.
19 S. Kajita, H. Washizu and T. Ohmori, *Phys. Rev. B: Condens. Matter Mater. Phys.*, 2010, **82**, 115424.
20 N. Sasaki, H. Okamoto, S. Masuda, K. Miura and N. Itamura, *Journal of Nanomaterials*, 2010, 742127.
21 Y. Guo, W. Guo and C. Chen, *Phys. Rev. B: Condens. Matter Mater. Phys.*, 2007, **76**, 155429.
22 C. Lee, Q. Li, W. Kalb, X.-Z. Liu, H. Berger, R. Carpick and J. Hone, *Science*, 2010, **328**, 76–80.
23 C. Lee, X. Wei, Q. Li, R. Carpick, J. W. Kysar and J. Hone, *Phys. Status Solidi B*, 2009, **246**, 2562–2567.
24 T. Filleter and R. Bennewitz, *Phys. Rev. B: Condens. Matter Mater. Phys.*, 2010, **81**, 155412.